High-contrast imaging of protoplanetary disks

Boer, J. de

Chapter 5

Characterizing instrumental effects on polarization at a Nasmyth focus using NACO

Based on

Jozua de Boer, Julien H. Girard, Dimitri Mawet, Frans Snik, Christoph U. Keller and Julien Milli[1]

Abstract

We propose a new calibration scheme to determine the instrumental polarization (IP) and crosstalk induced by either the telescope or an instrument at Nasmyth focus. We measure the polarized blue sky at zenith with VLT/UT4/NACO for different NACO derotator and telescope azimuth angles. Taking multiple measurements after rotating both the instrument and the telescope with angles of 90° allows use to determine the IP and most crosstalk components separately for the telescope and the instrument. This separation of the Mueller matrices of UT4 and the NACO is especially important for measurements taken in the conventional polarimetric mode (field stabilized), because the rotation of the instrument with respect to M3 causes a variation in the IP and crosstalk throughout the measurement. The technique allows us to determine the IP with an accuracy of 0.4%, and constrain or determine lower or upper limits for most crosstalk

[1] Published in the proceedings of SPIE, 9147, 914787 (2014).

components. Most notably, the UT4 $U \rightarrow V$ crosstalk is substantially larger than theory predicts. An angular offset in NACO's half wave plate orientation is a possible source of systematic errors. We measure this offset to be $1.8^\circ \pm 0.5^\circ$.

5.1 Introduction

Polarimetry is a powerful tool in the field of high contrast imaging and the characterization of the physical properties of circumstellar matter. For the best performance of a polarimeter, it is of paramount importance to know how much of the measured polarization comes from the science target, and how much is created by the telescope and instrument itself. Especially during observations in 'field tracking' mode, where the instrument is allowed to rotate with respect to the telescope pupil, we can no longer consider the telescope and instrument to form one system with a fixed instrumental effect on polarization. The issue of telescope/instrument induced polarization (*Instrumental Polarization*, IP) and transfer of one polarization state to another (*crosstalk*) becomes more complicated in this observing mode, because it depends on the rotation between the two components. Therefore, both telescope and instrument need to be characterized individually. IP and crosstalk can be of the order of tens of percent (Witzel et al. 2011). With the commissioning of SPHERE (Beuzit et al. 2006) during 2014, two new polarimetric imagers are put at the Nasmyth focus of Unit Telescope 3 (UT3) of the Very Large Telescope (VLT): the visible light polarimeter SPHERE/ZIMPOL (Schmid et al. 2012) and SPHERE/IRDIS (Beuzit et al. 2006), which allows for polarimetry in the near infrared (NIR). Improving the accuracy requires efficient schemes for future characterization of the contribution of both UT and instrument on the measured polarization. Improved calibration schemes are also greatly beneficial for future extremely large telescopes and facilities (e.g. E-ELT, TMT, GMT).

During the recent years, NAOS-CONICA (Girard et al. 2010, Lenzen et al. 2003, Rousset et al. 2003) (NACO) has proven to be very successful with its polarimetric modes (Avenhaus et al. 2014, Canovas et al. 2013, Garufi et al. 2013, Norris et al. 2013, Quanz et al. 2013). NACO was decommissioned and removed from VLT/UT4 in September of 2013, but will be re-commissioned at VLT/UT1 during the second half of 2014. To get the best science results from both future and archival NACO data, we need an accurate characterization of the UT and NACO optics. Witzel et al. (2011, W11) have compared models to standard star observations to calibrate IP and crosstalk for both NACO and UT4 in Ks. De Juan Ovelar et al. (submitted) also used standard star observations to calibrate the IP in H and Ks, yet assume crosstalk between linear polarization states to be negligible. We have performed calibration measurements with NACO in

polarimetric mode during the last week of August 2013, using the polarized zenith skylight around sunset. Harrington et al. (2011, H11) have shown that if we assume the scattering of sunlight by the earth atmosphere to be dominated by single Rayleigh scattering events, we can use the skylight for accurate calibration of the telescope and instrument. We can use the a priori knowledge of the incident polarization angle, to align the system such that we can rule out specific crosstalk contributions, as is explained in Sec. 5.2. As pointed out by H11, this calibration light source also has the advantage that it does not require the sacrifice of valuable night time for calibration measurements.

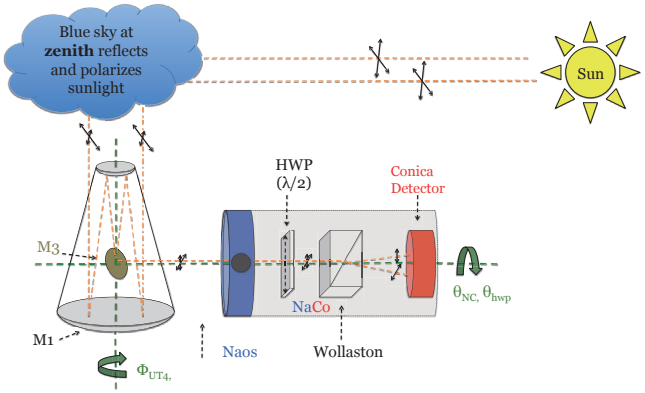

Figure 5.1: Schematic drawing of VLT/UT4 with NACO at the Nasmyth focus, based on Fig. 2 of W11. The green dashed lines with green arrows indicate the rotation axes of Φ_{UT4}, θ_{NC} and θ_{HWP}. The angles give the rotation of the optical system (or the polarization angle at the HWP), downstream from M1; NAOS; and HWP respectively.

For observations with NACO in polarimetric differential imaging (PDI) mode, a Wollaston prism splits the science beam into 2 orthogonally polarized beams: the *ordinary* (*o*), and *extra-ordinary* (*e*) beam. A field mask behind the Wollaston prevents overlap of both beams on the Conica detector. This creates a stripe pattern of the subsequent *o* and *e* beams that originate from the same area in the sky (see Fig. 5.2). Tinbergen (1996) and Canovas et al. (2011) describe the benefits of either the double difference or double ratio method for a dual beam analyzer. Combining the 4 beams of 2 half wave plate (HWP) positions 45° degrees apart, enables a correction for differences between the *o* and *e* beam created

by transmission and efficiency imperfections of the beam splitter. The principle of double difference is taken two steps further in this study. Besides rotating the HWP with 45°, we also rotate NACO with 90° on the derotator, and UT4 with 90° around the azimuth axis, as shown in Fig. 5.1) Each subsequent rotation allows us to correct for polarization effects induced by the instrument/telescope, downstream from the rotated optical component.

We can describe the polarization state of a beam of light with the use of the Stokes parameters: The total intensity (I); the horizontal linearly polarized intensity (Q, with $Q < 0$ for vertical polarization); the linearly polarized intensity in the 45° direction (U, with $U < 0$ for polarization in the 135° direction); and the right-handed circularly polarized intensity (V, $V < 0$ for left-handed). The 4 Stokes vector components

$$S = [I, Q, U, V]^T, \tag{5.1}$$

of the light receding from the i^{th} optical component S_{out} can be related with the incoming stokes vector S_{in} according to

$$S_{out} = M_i \cdot S_{in}, \tag{5.2}$$

with M_i the 4×4 Mueller matrix for the i^{th} optical component.

$$M_i = \begin{pmatrix} I \to I & Q \to I & U \to I & V \to I \\ I \to Q & Q \to Q & U \to Q & V \to Q \\ I \to U & Q \to U & U \to U & V \to U \\ I \to V & Q \to V & U \to V & V \to V \end{pmatrix}. \tag{5.3}$$

The aim of this study is to empirically determine the components of this Mueller matrix for both UT4 (M_{UT4}) and NACO (M_{NC}). The first ($I \to I$) component of this matrix describes the transmittance of i. IP is described by the lower 3 components of the first column. Crosstalk is described by all 9 components remaining after the exclusion of the first row and the first column. The remaining 3 elements of the first row ($Q, U, V \to I$) are best described as the influence of polarized signals on the photometry. Due to the similar design, M_{UT1} (NACO's future UT) and M_{UT3} (UT SPHERE) are expected to largely resemble M_{UT4} (NACO's previous UT), as long as we consider the same wavelength range. However, small differences might occur in time, caused by the difference of the aluminum oxide layers grown on the UT mirrors after each subsequent re-aluminization (van Harten et al. 2009).

In Sec. 5.2, we describe the underlying principles of our calibration scheme, and the default instrumental setup used. It is from this starting point that we will rotate the different optical components to perform the calibration measurements. These measurements and the data reduction are described in Sec. 5.3. Our results will be given in the form of Mueller matrices for both NACO and UT4 in Sec. 5.4. The outcome is discussed together with an outlook for this study in Sec. 5.5.

5.2 Calibration principles

We aim to retrieve the individual Mueller matrices for both UT4 (M_{UT4}) and NACO (M_{NC}). Combining both Mueller matrices relates the stokes vector for the light that reaches the Conica detector to the incident sky light according to:

$$S_{meas} = T(-p) \cdot M_{NC} \cdot M_{UT4} \cdot T(p) \cdot S_{sky}, \tag{5.4}$$

where $T(p)$ is the rotation matrix of Eq. 5.37, accounting for the paralactic angle p of the telescope pointing.

5.2.1 Default instrumental setup

Most studies (H11, W11) let the reference frame for the polarization angle (i.e. coordinate axes for $\pm Q$) be determined by the meridian. We choose the reference frame to be fixed to reflection plane of the third mirror (M3) of UT4. This choice allows us to ignore $T(p)$ in Eq. 5.4, but instead consider the incident S_{sky} to have changed for a different telescope pointing. We consider light to be horizontally polarized, when it is linearly polarized perpendicular to the M3 reflection plane, and vertical when the light is polarized perpendicular to both this horizontal direction and the propagation direction of the beam. We consider the following as our default setup:

- We observe sunlight that is polarized by scattering in the terrestrial atmosphere;
- UT4 is pointing at zenith, with an azimuth angle opposite to the sun: $\Phi_{UT4} = \Phi_{\odot} + 180^{\circ} = 0$;
- NACO is oriented such that the first mirror of Naos (M4) reflects the light in a plane perpendicular to the relection plane of M3. For this rotator angle of NACO, $\theta_{NC} = 0$;
- The fast axis of NACO's half wave plate retarder (HWP) is aligned with the polarization angle of the o beam: $\theta_{hwp} = 0$.

The Rayleigh scattered sunlight will be partially linearly polarized (to a variable, and therefore unknown degree) in the (very well known) direction orthogonal to the scattering plane in the sky (i.e. the principal plane). Skylight does not have a circular polarization component. Having $\Phi_{UT4} = \Phi_{\odot} + 180^{\circ}$ will place the M3 reflection plane orthogonal with the principal plane. This yields the following incident sky Stokes vector for the default instrumental setup:

$$S_{sky} = [I_{sky}, -Q_{sky}, 0, 0]^T. \tag{5.5}$$

If $(i_o - i_e)|_{\theta_{HWP}}$ is the difference between the measured intensity of the o and e beams for a given θ_{HWP}, the classical double difference method (Canovas et al. 2011) can be described as:

$$\begin{aligned} Q_{meas}[\theta_{HWP}] &= 0.5((i_o - i_e)|_{0^\circ} - (i_o - i_e)|_{45^\circ}) && (5.6)\\ &= -Q_{trans} + Q_{UT4} + Q_{NC}, && (5.7)\end{aligned}$$

with Q_{trans} the transmitted Q_{sky}; Q_{UT4} is the (by NACO transmitted) UT4 induced IP, and + Q_{NC} the NACO induced IP and ($[U, V]_{UT4} \rightarrow Q_{NC}$) crosstalk:

$$\begin{aligned} Q_{trans} &= M_{NC}[2,2] \times M_{UT4}[2,2] \times Q_{sky}, && (5.8)\\ Q_{UT4} &= M_{NC}[2,2] \times M_{UT4}[2,1] \times I_{sky}, && (5.9)\\ Q_{NC} &= M_{NC}[2,1] \times \mathbf{I}_{UT4} + M_{NC}[2,3] \times \mathbf{U}_{UT4} + M_{NC}[2,4] \times \mathbf{V}_{UT4}, && (5.10)\end{aligned}$$

with $(\mathbf{I}, \mathbf{U}, \mathbf{V})_{UT4}$ the respective S_{out} parameters of UT4, incident to NACO. $M_{UT4}[2,2]$ and $M_{NC}[2,2]$ are related to the $Q \rightarrow Q$ components of UT4 and NACO respectively. These components can be calibrated with a source of known Degree of Linear Polarization (DoLP = $\sqrt{Q^2 + U^2}/I$), such as a polarized standard star. Doing so falls outside the scope of the current study, but will be included in future work. However, these components are expected to be very close to unity, which we will therefore assume below.

The corresponding intensity I is determined by:

$$I_{meas}[\theta_{HWP}] = 0.5((i_o + i_e)|_{0^\circ} + (i_o + i_e)|_{45^\circ}). \quad (5.11)$$

5.2.2 Deriving UT4 instrumental polarization: Q_{UT4}

We extend the double difference principle by combining a measurement in the default setup (= Q_1) with one where $\theta_{NC} = 90^\circ$ (= Q_2). Just as Eq. 5.6 corrects for transmission difference between the o and e beam, a $\theta_{NC} = 0, 90^\circ$ double difference allows us to correct for NACO's contribution to the IP (but not crosstalk), as was suggested by W11:

$$Q_2 \approx -Q_{trans} + Q_{UT4} - Q_{NC}. \quad (5.12)$$

We combine Eq. 5.7 and 5.12 with Eq. 5.10 to get

$$Q_A = (Q_1 + Q_2)/2 = -Q_{trans} + Q_{UT4} + M_{NC}[2,3] \times \mathbf{U}_{UT4}, \quad (5.13)$$

with

$$\mathbf{U}_{UT4} = M_{UT4}[3,1] \times I_{sky} + M_{UT4}[3,2] \times -Q_{sky}. \quad (5.14)$$

To determine the IP of UT4, we can apply the same strategy of rotating the instrumental component that is to be corrected for. In this case, the strategy implies that we have to rotate the telescope itself with respect to the sky. Because we are looking at zenith, we will still point at the same part of the sky after changing the telescope azimuth to $\Phi_{UT4} = 90°$. Since we decided to use the scattering plane of M3 as a reference, this changes the incident stokes vector from Eq. 5.5 to $S_{sky} = [I_{sky}, Q_{sky}, 0, 0]^T$. Repeating the two previous measurements for the new azimuth position gives:

$$Q_3 = Q_{trans} + Q_{UT4} + Q_{NC}, \tag{5.15}$$

$$Q_4 = Q_{trans} + Q_{UT4} - Q_{NC}, \tag{5.16}$$

$$Q_B = (Q_3 + Q_4)/2 = Q_{trans} + Q_{UT4} - M_{NC}[2,3] \times \mathbf{U}_{UT4}. \tag{5.17}$$

The changing sign of $\mathbf{U}_{UT4}$ is caused by the changing sign of Q_{sky}, and the assumption that $M_{UT4}[3,1] = 0$, as is proposed by W11 and H11. This allows us to retrieve the UT4 induced IP according to:

$$Q_{UT4} = (Q_A + Q_B)/2 \tag{5.18}$$

5.2.3 From measurements to matrix components

We assume our pointing to be perfect, meaning that our light incident to our telescope is either $S_{sky} = [I, \pm Q, 0, 0]^T$ (Aug. 31), or $S_{sky} = [I, 0, \pm U, 0]^T$ (Sep. 1). In Tabs. 5.3 and 5.5 of Appendix 5.B, we list the different transmission, instrumental polarization and crosstalk components measured with the setups listed in Tabs. 5.2 and 5.4 of Appendix 5.B. Just as we did in the previous section for Q_{UT4}, we can use the sign changes of the listed components for different instrumental setups. This sign change allows us to isolate the components by adding and subtracting the individual measurements. From Tab. 5.3, we can find that from the 16 $X_{sky} \rightarrow X_{UT4} \rightarrow X_{NC}$ components of the Q_{1-4} measurements, we can isolate 8 pairs of components:

$$(I \rightarrow I \rightarrow Q, U) + (I \rightarrow V \rightarrow Q, U) = [+Q, U_1 - Q, U_2 + Q, U_3 - Q, U_4]/4, \tag{5.19}$$

$$(I \rightarrow Q \rightarrow Q, U) + (I \rightarrow U \rightarrow Q, U) = [+Q, U_1 + Q, U_2 + Q, U_3 + Q, U_4]/4, \tag{5.20}$$

$$(Q \rightarrow I \rightarrow Q, U) + (Q \rightarrow V \rightarrow Q, U) = [-Q, U_1 + Q, U_2 + Q, U_3 - Q, U_4]/4, \tag{5.21}$$

$$(Q \rightarrow Q \rightarrow Q, U) + (Q \rightarrow U \rightarrow Q, U) = [-Q, U_1 - Q, U_2 + Q, U_3 + Q, U_4]/4, \tag{5.22}$$

where Eq. 5.20 is the same Eq. 5.18 and is what we called the UT4 $I \rightarrow Q$ instrumental polarization. For each equation above, Q, U means either Q or U. Similarly, from the 16 measurements listed in Tab. 5.5 we can isolate the following 8 pairs of components:

$$(I \rightarrow I \rightarrow Q, U) + (I \rightarrow V \rightarrow Q, U) = [+Q, U_5 - Q, U_6 + Q, U_7 - Q, U_8]/4, \quad (5.23)$$

$$(I \rightarrow Q \rightarrow Q, U) + (I \rightarrow U \rightarrow Q, U) = [+Q, U_5 + Q, U_6 + Q, U_7 + Q, U_8]/4, \quad (5.24)$$

$$(U \rightarrow I \rightarrow Q, U) + (U \rightarrow V \rightarrow Q, U) = [+Q, U_5 - Q, U_6 - Q, U_7 + Q, U_8]/4, \quad (5.25)$$

$$(U \rightarrow Q \rightarrow Q, U) + (U \rightarrow U \rightarrow Q, U) = [+Q, U_5 + Q, U_6 - Q, U_7 - Q, U_8]/4. \quad (5.26)$$

5.3 Observations and data reduction

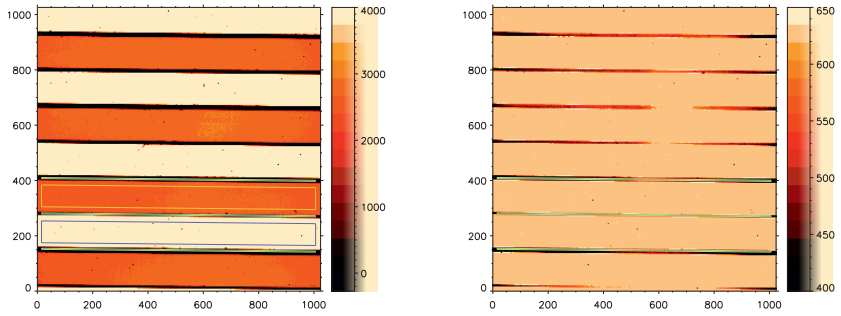

Figure 5.2: Left: Example of the o and e stripe pattern accross the detector, with dark masked areas in between. The mean pixel values in the blue and yellow boxes are respectively i_o and i_e in Eq. 5.6. **Right:** NACO detector image, with a dynamic range chosen to show the masked regions. This dynamic range shows that stray light has contaminated both the masked and unmasked regions alike. The 3 green boxes in the masked areas are used to determine the stray light correction of Sec. 5.3.3.

5.3.1 IP and crosstalk calibration observations

We have observed the sky light just before and after sunset at both the 31^{st} of August, and the 1^{st} of September of 2013. All our observations have been performed in the H band, have (NDIT =) 2 exposures of 4 seconds. Appendix 5.B lists the observations and their changes with respect to the default instrumental setup of Sec. 5.2.1.

The 31^{st} of August, we have observed the sky with an incident polarization angle at either 0° or 90° with respect to the reference frame of UT4. We observed around sunset, when the intensity of the sky light decreases quickly, while the DoLP increases, even beyond the 90° scattering angle of sunset. For each UT4/NACO position, Q and U are measured using a set of 4 HWP positions according to the double difference method of Eq. 5.6: $\theta_{HWP} = [0, 45, 22.5, 67.5]$. These sets of HWP angles are repeated for all 4 possible UT4/NACO combinations, rotating either or both UT4 and NACO with 90°. The HWP set is repeated for the first (= default) UT4/NACO position to allow us to correct for changing sky conditions. The resulting 5 HWP sets are listed in Tab. 5.2.

The evening of the 1^{st} of September, the sky polarization angle was at either +45° or −45° compared to the M3 reflection plane. This time, we have performed the entire sequence two times, for a better correction of the change of incident polarization and intensity. The observations taken this evening are listed in Tab. 5.4.

During the observations, the sun moved accross the sky. The changing solar azimuth position creates a small uncertainty in the polarization angle of $\Delta\Phi_{\odot} = 1°$. The decreasing altitude, accounts for a large change in incident DoLP, as is discussed in Sec. 5.3.3.

5.3.2 HWP angle offset calibration observations

On the 1^{st} of September 2013, we have observed the Zenith sky in the default instrumental setup, for 16 different HWP angles, with intervals of 11.25°.

5.3.3 Data reduction

After we take the mean of the two individual exposures (DITS) per HWP angle, A thermal background or *dark* measurement is subtracted from this mean sky frame. The sky frame is divided by a normalized sky flatfield, the latter taken without the Wollaston. The lefthand image of Fig. 5.2 shows the resulting sky frame, from which we select one large area (994 × 80 pixels) in both an *o* beam stripe (blue box), and an *e* beam stripe (yellow box).

Stray light is visible as a brighter band running diagonally accross the detector, from the top (right from center) to the bottom center. The righthand

image shows the same frame, for the value range of 525 ± 125 counts, which are the mean values of the areas masked by the Wollaston mask of NACO. Ideally, the values of the masked regions should on average be zero after dark subtraction. However, we can clearly see the same stray light band run accross the masked region. To correct for this stray light, each pixel column of the boxed areas of interest are corrected in the following way: We determined the mean value of five masked pixels above, and five masked pixels below both the *o* and *e* boxes of interest (indicated by the 3 green boxed areas in the righthand image of Fig. 5.2), and subtract this value from the corresponding pixel columns of the *o* and *e* boxes.

We correct for dead or hot pixels by replacing each pixel which has a value deviating from the mean with more than 3 sigma, with the median value of its surrounding pixels. i_o and i_e of Eq. 5.6 are in fact the mean pixel value for the *o* and *e* box respectively.

Changing sky conditions

During the cycle of observations the solar altitude decreases, leaving neither the intensity, nor the polarization of the sky light constant. For this study we have used the simple assumption of a linearly increasing DoLP with time, which is the consequence of single Rayleigh scattering (Harrington et al. 2011). The repetition of an identical set of measurements at the beginning and at the end of the cycle allows us to determine the slope of the polarized fraction. We have corrected all measured values for the average increase of the polarized fraction of datapoints with identical instrumental setup. Fig. 5.3 shows the fractional polarization for the measurements taken on the 1^{st} of September, before and after correction for changing sky polarization.

Double difference: 2 half wave plate angles

The double difference values are determined according to Eq. 5.6, and divided by I. In Fig. 5.4, we plot the absolute values of the double difference divided by I against the measurement time. Fig. 5.4 plots the absolute value to illustrate the fluctuations in the measured values of $(Q, U)_{meas}/I_{meas}$ for the different instrumental setups (described in the legend). Keep in mind that our equations of Sec. 5.2 do not use the absolute values.

Double difference: 2 NACO derotator angles

The first 4 $(Q/I)_{meas}$ (> 0.5) values of the $S_{sky} = [I, \pm Q, 0, 0]^T$ measurements of Fig. 5.4 are in fact Q_{1-4} of Sec. 5.2.2, albeit not in the same order. Due to our choice

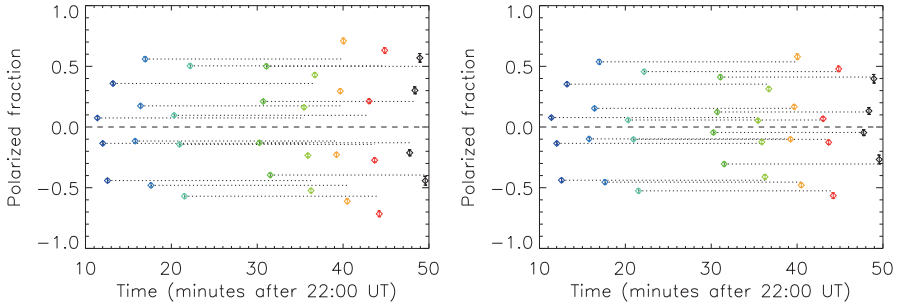

Figure 5.3: Fractional polarization of the September 1 measurements (Tab. 5.4) plotted against time (minutes after 22:00 UTC = 6 p.m. local time) **Left:** Before correcting for the increasing sky polarization. **Right:** After correcting for increasing sky polarization. The horizontal dotted lines connect the datapoints with the same instrumental setup. Given ideal conditions (i.e. time constant S_{in}), two datapoints on either side of the horizontal lines, would have the same fractional polarization. The colors represent the different instrumental setups, explained in the legends of Fig. 5.4

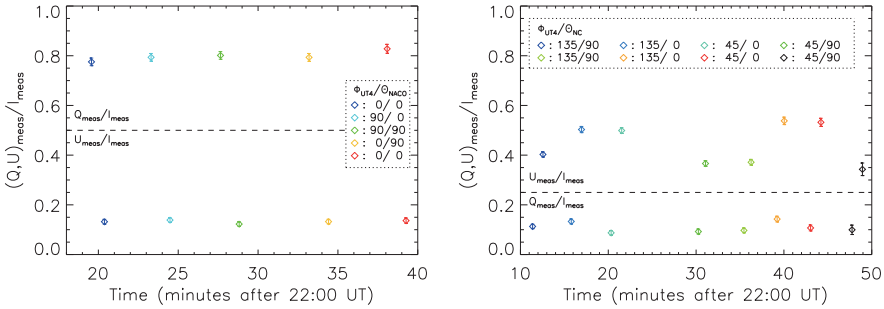

Figure 5.4: The absolute values of the classical double difference: combining 2 measurement with HWP angles 45° apart to determine $|Q, U|_{meas}/I_{meas}$. **Left:** August 31 measurements with $S_{sky} = [I, \pm Q, 0, 0]^T$. Without exception: $|Q/I|_{meas} > 0.5$, and $|U/I|_{meas} < 0.5$. **Right:** September 1 measurement with $S_{sky} = [I, 0, \pm U, 0]^T$. Without exception: $|Q/I|_{meas} < 0.25$, and $|U/I|_{meas} > 0.25$.

of reference frame, $Q_{A,B}$ of Eqs. 5.13 and 5.17 are a second example of the double difference technique. This time, instead of combining different HWP angles, we combine measurements taken before and after a rotation of NACO of 90°. With this double difference we cancel out $M_{NC}[2,1] \times \mathbf{I}_{UT4}$ and $M_{NC}[2,4] \times \mathbf{V}_{UT4}$ of Eq. 5.10.

5.4 Results

5.4.1 NACO HWP offset

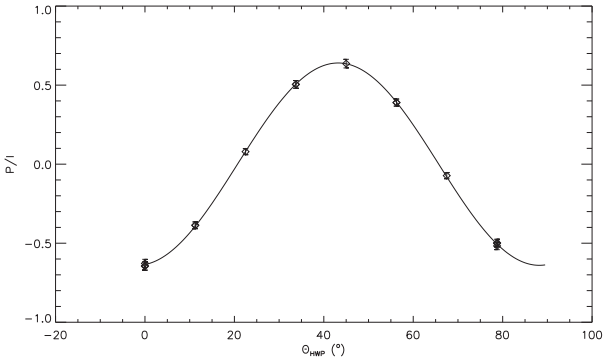

Figure 5.5: Polarized fraction plotted against the angle of the half wave plate, as given by the FITS header. The solid line is a best fit $-\cos(2\theta_{HWP} + \phi_{HWP})$, with an offset angle of $\phi_{HWP} = 1.8° \pm 0.5°$.

The offset between the fast axis of NACO's half wave plate and the angle given in the driver software and image headers has been much debated in literature. Witzel et al. (2010, W10) report that the angle between the reference system and the HWP fast axis was as large as $-6.6 \pm 0.2°$. According to the 2009 NACO intervention report, the zero-encoder position is "set to zero". There is no mention in the report what the angular change is with respect to the pre-2009 position. However, W11 state that the difference of the revision is this very 6.6°. In other words, it does not have to be taken into account for measurements after 2009.

Various authors have used the warning by W10 as an argument to take a HWP offset into account. Garufi et al. (2013) and Avenhaus et al. (2014) fit the offset angle for each dataset. Our calibration scheme is based on the

assumption of a known angle of the sky polarization. For large HWP angular offsets we would need to correct Eqs. 5.19 to 5.26. We therefore calibrated the HWP offset by measuring the polarized fraction for different HWP angles, with $\Delta\theta_{HWP} = 11.25$, which we plotted in Fig. 5.5. We have fitted the data to:

$$A_0 \cos(\theta_{HWP} - \phi_{HWP}) = A_1 \sin(\theta_{HWP}) + A_2 \cos(\theta_{HWP}), \tag{5.27}$$

where A_1 and A_2 are determined with a linear regression. From this, we can constrain the constants A_0 and ϕ_{HWP} according to:

$$(Q/I)_{sky} \approx A_0 = \sqrt{A_1^2 + A_2^2}, \tag{5.28}$$

$$\phi_{HWP} = \arctan(A_1/A_2). \tag{5.29}$$

The best fit yields an offset of $\phi_{HWP} = 1.8° \pm 0.5°$, where the error is dominated by the uncertainty in the solar azimuth angle of 1°. This HWP offset is responsible for a measurement error < 0.0016, much smaller than the random error in our measurements (see Tab. 5.1). Based on this result, we have ignored any error caused by the HWP offset.

5.4.2 Matrix components

Table 5.1: Results of Eqs. 5.19 to 5.26, based on sky observations taken at the 31st of August (3rd column) and the 1st of September (5th column), 2013.

Component	Eq.	Result	Eq.	Result	Constraining
$(I \to I \to Q) + (I \to V \to Q)$	5.19	-0.004 ± 0.008	5.23	-0.008 ± 0.004	$M_{NC}[2,1]$
$(I \to I \to U) + (I \to V \to U)$	5.19	-0.003 ± -0.008	5.23	-0.007 ± 0.004	$M_{NC}[3,1]$
$(I \to Q \to Q) + (I \to U \to Q)$	5.20	-0.006 ± 0.008	5.24	-0.013 ± 0.004	$M_{UT4}[2,1]$
$(I \to Q \to U) + (I \to U \to U)$	5.20	-0.016 ± 0.008	5.24	0.010 ± 0.004	$M_{UT4}[2,1] * M_{NC}[3,2]$
$(Q \to I \to Q) + (Q \to V \to Q)$	5.21	-0.008 ± 0.008			not significant
$(Q \to I \to U) + (Q \to V \to U)$	5.21	-0.0003 ± 0.008			not significant
$(Q \to Q \to U) + (Q \to U \to U)$	5.22	-0.114 ± 0.008			$M_{NC}[3,2]$
$(U \to I \to Q) + (U \to V \to Q)$			5.25	-0.009 ± 0.004	$M_{NC}[2,4]$
$(U \to I \to U) + (U \to V \to U)$			5.25	0.074 ± 0.004	$M_{NC}[3,4]$
$(U \to Q \to Q) + (U \to U \to Q)$			5.26	-0.107 ± 0.004	$M_{NC}[2,3]$

We have listed the measured results of Eqs. 5.19 to 5.26 under "Result" in Tab. 5.1. As can be seen from the equations under "Component", the result reflects de facto multiple matrix components. However, the M_{UT4} and/or M_{NC} components which are most constrained by the result, are listed in the column "Constraining". This does not always mean that this matrix component is the same as the measured result. For example, to determine $M_{NC}[2,4]$ from the result of Eq. 5.25, the result has to be divided by both U_{sky} and $M_{UT4}[4,3]$.

5.4.2.1 UT4 Mueller matrix components

The "Constraining' column of Tab. 5.1 only holds one value for M_{UT4}, namely the [2, 1] component, determined from the mean of Eqs. 5.20 and 5.24. We know that due to the symmetry in M1 and M2, neither of these mirrors should contribute to M_{UT4}. We can therefore consider $M_{UT4} = M_{M3}$. For a one mirror matrix, we can assume that it is symmetric around the diagonal, and compute the remaining values using the Fresnel equations (van Harten et al. 2009, W11), with the refractive indices for aluminum in H band being $R_\perp = 0.98308$; $R_\parallel = 0.96644$ and its reflection phase for a 45° angle of incidence are $\phi_\perp = -175.108°$; $\phi_\parallel = -170.215°$ [1]. The resulting Mueller matrix for $UT4$ is:

$$M_{UT4} = \begin{pmatrix} 1 & -0.010 \pm 0.004 & 0 & 0 \\ -0.010 \pm 0.004 & 1 & 0 & 0 \\ 0 & 0 & -0.996 & -0.0853 \\ 0 & 0 & 0.0853 & -0.996 \end{pmatrix}. \tag{5.30}$$

The black values in Eq. 5.30 represent the ones determined from the results in Tab. 5.1, whereas the blue values are computed from the Fresnel equations.

5.4.2.2 NACO Mueller matrix components

Once we have determined M_{UT4}, we can determine the values from M_{NC}. Because NACO IP and crosstalk is not determined by multiple reflections and transmissions, we can no longer assume the matrix to be symmetric. Therefore, we have assumed the values for the first row of M_{NC}, which hardly influence our measurements, and ignored the last row, which NACO cannot measure.

$$M_{NC} = \begin{pmatrix} 1 & 0 & 0 & 0 \\ -0.006 \pm 0.004 & 1 & 0.160 \pm 0.068 & -0.170 \pm 0.058 \\ -0.005 \pm 0.004 & 0.147 \pm 0.071 & -0.662 \pm 0.338 & \mathbf{1.31} \\ - & - & - & - \end{pmatrix}. \tag{5.31}$$

Once again, the black values in Eq. 5.31 are determined from the results listed in Tab. 5.1. The red values are components that still have to be changed, due to the considerations below. The large uncertainties on the [2, 3], [2, 4] and [3, 4] components are caused by the large uncertainty of our U_{sky}, by which we have to divide the results of Tab. 5.1 to determine the corresponding matrix components. This uncertainty is in turn created by our lack of knowledge of component [3, 3].

[1] Refractive indices and reflection phases are obtained from *www.RefractiveIndex.INFO*.

If we assume $M_{NC}[3,3] = 1$, then $(U/I)_{sky} = M_{UT4}[3,3] \times 0.442 = 0.996 \times 0.442 = 0.440$, but this is not likely to be the case. Therefore, we have used this value as a lower limit of $(U/I)_{sky}$, and used the highest Q_{meas} value of 0.9 as an upperlimit: $(U/I)_{sky} = 0.670 \pm 0.230$, and $M_{NC}[3,3] = 0.662 \pm 0.338$.

We are left with a non-physical value for $M_{NC}[3,4]$ = (result of Eq. 5.25) $/(U/I)_{sky}/[4,3]_{UT}$, which becomes $0.074/0.662/0.0853 = 1.31$. This means that there must be an error in our assumptions, both of which would be quite surprising:

- $M_{UT4}[1,3] \neq 0$
- $M_{UT4}[4,3] >> 0.0853$

Besides bringing down the value for $M_{NC}[2,4]$, changing either would impact at least $M_{NC}[2,4]$, $M_{NC}[2,2]$, and $M_{UT4}[3,3]$. Finding the optimal solution is best done iteratively, which we leave for future studies. Below, we discuss a very coarse analysis of either proposed solution for the non-physicality of the $V \rightarrow U$ crosstalk of Naco.

Substantial UT4 $U \rightarrow I$ component

If we don't change any of the other components, the most extreme case, with $M_{UT4}[1,3] = 1$ yields:

$$M_{NC}[3,4] = (0.074 + 0.670 \times -0.005)/(0.670 \times 0.085) = 1.240. \quad (5.32)$$

Since $M_{NC}[3,4] > 1$, we can conclude that this option does not solve the problem.

Larger UT4 $U \rightarrow V$ crosstalk

A solution for:

$$M_{NC}[3,4] = 0.074/(0.670 \times M_{UT4}[4,3]) < 1, \quad (5.33)$$

can be found for $0.11 < M_{UT4}[4,3] < 1$, which yields $1 > M_{NC}[3,4] > 0.11$. This provides lower limits for the new Mueller matrices:

$$M_{UT4} = \begin{pmatrix} 1 & -0.010 \pm 0.004 & 0 & 0 \\ -0.010 \pm 0.004 & 1 & 0 & 0 \\ 0 & 0 & > -0.994 & < -0.110 \\ 0 & 0 & > 0.110 & > -0.994 \end{pmatrix}, \quad (5.34)$$

and

$$M_{NC} = \begin{pmatrix} 1 & 0 & 0 & 0 \\ -0.006 \pm 0.004 & 0.983 \pm 0.017 & 0.161 \pm 0.068 & > -0.122 \\ -0.005 \pm 0.004 & 0.147 \pm 0.071 & -0.662 \pm 0.338 & > 0.110 \\ - & - & - & - \end{pmatrix}. \quad (5.35)$$

The $M_{NC}[2,2]$ value is determined by normalizing the last three values of the second row according to $[2,2] = \sqrt{[2,3]^2 + [2,4]^2}$. In the same way, we have determined $M_{UT4}[3,3]$.

5.5 Discussion and outlook

We present the preliminary constraints on the Mueller matrices for UT4 and NACO. These matrix values are obtained by observing the polarized blue sky at zenith, while rotating both UT4 and NACO with 90° angles, as described in Sec. 5.2. Despite the large error bars for some matrix components of Eqs. 5.34 and 5.35, or that we could only determine upper or lower limits for other components, this study is an important first step for a more accurate determination of the effects of the telescope and NACO on the measured polarization. We find that the UT4 $U \rightarrow V$ crosstalk is substantially larger than theory predicts, which might be explained by the existance of an aluminium-oxide coating of M3 (van Harten et al. 2009).

To the best or our knowledge, for neither NACO, nor UT4, complete Mueller matrices are published for the H band. W11 have determined the full M_{NC} for the Ks band, with the use of standard star observations. The advantage of our calibration method is that it can be performed without using valuable night time. De Juan Ovelar et al. (submitted) determined the IP for both H and Ks band. They find $I \rightarrow Q_{NC} = -0.024$, which is 4 times higher than our value of -0.006, but their $I \rightarrow U_{NC} = -0.005$ is in good agreement with our value. The difference between their H and Ks values teaches us that a direct comparison between our M_{NC}(H) and the M_{NC}(Ks) of W11 is not valid. The mueller matrix appears to be too color dependent to do so.

For our matrices to be useful for the correction of astrophysical data, we need to determine especially $M_{NC}[3,3]$ with higher precision. We intend to constrain this value further with the use of standard star observations. Furthermore, H11 have demonstrated that a normal non-linear least-squares minimalization can be applied to determine the Mueller matrix values. The next step in our study will be to apply this least squares method as a further refinement of our calibration.

Acknowledgements

JdB acknowledges ESO for its support provided with the studentship program. We furthermore thank ESO staff of the Paranal Observatory for their support during the observations, especially Fernando Salgado.

5.A Appendix: Rotational (a)symmetry of Mueller matrix components

Whether rotating an element by 90° changes the sign of the IP or crosstalk component, depends on whether the rotation occurs upstream or downstream from the reference frame. Rotating the component fixed to the reference plane is equal to rotating the polarization angle of the incident light (i.e. upstream rotation):

$$M_{upstream\_rot=90^\circ} = M \cdot T(90^\circ) = \begin{pmatrix} + & - & - & + \\ + & - & - & + \\ + & - & - & + \\ + & - & - & + \end{pmatrix}, \tag{5.36}$$

with $T(90^\circ)$ the rotation matrix (W11):

$$T(p) = \begin{pmatrix} 1 & 0 & 0 & 0 \\ 0 & \cos(2p) & \sin(2p) & 0 \\ 0 & -\sin(2p) & \cos(2p) & 0 \\ 0 & 0 & 0 & 1 \end{pmatrix}. \tag{5.37}$$

A + sign in Eq. 5.36 indicates that the matrix component does not change sign with rotation whereas a − sign means that the matrix component does change sign. Notice that I_{in} and V_{in} do not change with rotation. Therefore, the signs of the matrix components of the first and last column remain unchanged.

Rotating the optical system downstream from the reference frame gives a different behaviour, because we need an additional $T(-90^\circ)$ in the equation to get back to our initial reference frame. In this case, the change of sign occurs for the elements where a Stokes component insensitive to rotation (I, V) is transformed in a Stokes component that is (Q, U), or vice versa:

$$M_{downstream\_rot=90^\circ} = T(-90^\circ) \cdot M \cdot T(90^\circ) \begin{pmatrix} + & - & - & + \\ - & + & + & - \\ - & + & + & - \\ + & - & - & + \end{pmatrix}. \tag{5.38}$$

5.B Appendix: Observation tables

Table 5.2: Sky observations taken at the 31st of August 2013. All coordinates are given as changes with respect to the default instrumental setup of Sec. 5.2.1.

Universal Time	$\Phi_{UT4}(^\circ)$	$\theta_{NC}(^\circ)$	$\theta_{HWP}(^\circ)$	$(Q,U)_{1-4}$
22:19:34.2	0	0	0	Q_1
22:20:00.8	0	0	45	Q_1
22:20:22.9	0	0	22.5	U_1
22:20:49.5	0	0	67.5	U_1
22:23:18.1	90	0	0	Q_3
22:23:55.9	90	0	45	Q_3
22:24:29.1	90	0	22.5	U_3
22:25:06.8	90	0	67.5	U_3
22:27:39.0	90	90	0	Q_4
22:28:16.6	90	90	45	Q_4
22:28:49.0	90	90	22.5	U_4
22:29:27.3	90	90	67.5	U_4
22:33:11.6	0	90	0	Q_2
22:33:51.6	0	90	45	Q_2
22:34:24.8	0	90	22.5	U_2
22:35:02.5	0	90	67.5	U_2
22:38:05.2	0	0	0	Q_1
22:38:42.8	0	0	45	Q_1
22:39:16.0	0	0	22.5	U_1
22:39:54.8	0	0	67.5	U_1

Table 5.3: A list of the compenents we measure with the different instrumental setups of Tab. 5.2. All components are listed in the form $X_{sky} \rightarrow X_{UT4} \rightarrow X_{NC}$, but we do not state the subscripts.

$Q_1 =$	$+(I \rightarrow I \rightarrow Q)$	$+(I \rightarrow Q \rightarrow Q)$	$+(I \rightarrow U \rightarrow Q)$	$+(I \rightarrow V \rightarrow Q)$
	$-(Q \rightarrow I \rightarrow Q)$	$-(Q \rightarrow Q \rightarrow Q)$	$-(Q \rightarrow U \rightarrow Q)$	$-(Q \rightarrow V \rightarrow Q)$
$Q_2 =$	$-(I \rightarrow I \rightarrow Q)$	$+(I \rightarrow Q \rightarrow Q)$	$+(I \rightarrow U \rightarrow Q)$	$-(I \rightarrow V \rightarrow Q)$
	$+(Q \rightarrow I \rightarrow Q)$	$-(Q \rightarrow Q \rightarrow Q)$	$-(Q \rightarrow U \rightarrow Q)$	$+(Q \rightarrow V \rightarrow Q)$
$Q_3 =$	$+(I \rightarrow I \rightarrow Q)$	$+(I \rightarrow Q \rightarrow Q)$	$+(I \rightarrow U \rightarrow Q)$	$+(I \rightarrow V \rightarrow Q)$
	$+(Q \rightarrow I \rightarrow Q)$	$+(Q \rightarrow Q \rightarrow Q)$	$+(Q \rightarrow U \rightarrow Q)$	$+(Q \rightarrow V \rightarrow Q)$
$Q_4 =$	$-(I \rightarrow I \rightarrow Q)$	$+(I \rightarrow Q \rightarrow Q)$	$+(I \rightarrow U \rightarrow Q)$	$-(I \rightarrow V \rightarrow Q)$
	$-(Q \rightarrow I \rightarrow Q)$	$+(Q \rightarrow Q \rightarrow Q)$	$+(Q \rightarrow U \rightarrow Q)$	$-(Q \rightarrow V \rightarrow Q)$
$U_1 =$	$+(I \rightarrow I \rightarrow U)$	$+(I \rightarrow Q \rightarrow U)$	$+(I \rightarrow U \rightarrow U)$	$+(I \rightarrow V \rightarrow U)$
	$-(Q \rightarrow I \rightarrow U)$	$-(Q \rightarrow Q \rightarrow U)$	$-(Q \rightarrow U \rightarrow U)$	$-(Q \rightarrow V \rightarrow U)$
$U_2 =$	$-(I \rightarrow I \rightarrow U)$	$+(I \rightarrow Q \rightarrow U)$	$+(I \rightarrow U \rightarrow U)$	$-(I \rightarrow V \rightarrow U)$
	$+(Q \rightarrow I \rightarrow U)$	$-(Q \rightarrow Q \rightarrow U)$	$-(Q \rightarrow U \rightarrow U)$	$+(Q \rightarrow V \rightarrow U)$
$U_3 =$	$+(I \rightarrow I \rightarrow U)$	$+(I \rightarrow Q \rightarrow U)$	$+(I \rightarrow U \rightarrow U)$	$+(I \rightarrow V \rightarrow U)$
	$+(Q \rightarrow I \rightarrow U)$	$-(Q \rightarrow Q \rightarrow U)$	$-(Q \rightarrow U \rightarrow U)$	$+(Q \rightarrow V \rightarrow U)$
$U_4 =$	$-(I \rightarrow I \rightarrow U)$	$+(I \rightarrow Q \rightarrow U)$	$+(I \rightarrow U \rightarrow U)$	$-(I \rightarrow V \rightarrow U)$
	$-(Q \rightarrow I \rightarrow U)$	$+(Q \rightarrow Q \rightarrow U)$	$+(Q \rightarrow U \rightarrow U)$	$-(Q \rightarrow V \rightarrow U)$

Table 5.4: Sky observations taken at the 1st of September, 2013.

Universal Time	$\Phi_{UT4}(^\circ)$	$\theta_{NC}(^\circ)$	$\theta_{HWP}(^\circ)$	$(Q,U)_{5-8}$
22:11:23.2	135	90	0	Q_8
22:12:00.7	135	90	45	Q_8
22:12:33.9	135	90	22.5	U_8
22:13:12.1	135	90	67.5	U_8
22:15:47.4	135	0	0	Q_7
22:16:24.6	135	0	45	Q_7
22:16:57.4	135	0	22.5	U_7
22:17:37.4	135	0	67.5	U_7
22:20:19.7	45	0	0	Q_5
22:20:56.9	45	0	45	Q_5
22:21:31.8	45	0	22.5	U_5
22:22:11.0	45	0	67.5	U_5
22:30:15.5	45	90	0	Q_6
22:30:42.4	45	90	45	Q_6
22:31:04.5	45	90	22.5	U_6
22:31:31.2	45	90	67.5	U_6
22:35:27.0	135	90	0	Q_8
22:35:53.8	135	90	45	Q_8
22:36:15.8	135	90	22.5	U_8
22:36:42.5	135	90	67.5	U_8
22:39:13.7	135	0	0	Q_7
22:39:40.5	135	0	45	Q_7
22:40:02.5	135	0	22.5	U_7
22:40:29.3	135	0	67.5	U_7
22:43:02.0	90	0	0	Q_5
22:43:40.7	90	0	45	Q_5
22:44:12.9	90	0	22.5	U_5
22:44:50.8	90	0	67.5	U_5
22:47:45.5	45	90	0	Q_6
22:48:22.1	45	90	45	Q_6
22:48:56.3	45	90	22.5	U_6
22:49:34.3	45	90	67.5	U_6

Table 5.5: A list of the compenents we measure with the different instrumental setups of Tab. 5.4. All components are listed in the form $X_{sky} \rightarrow X_{UT4} \rightarrow X_{NC}$, but we do not state the subscripts.

$Q_5 =$	$+(I \rightarrow I \rightarrow Q)$	$+(I \rightarrow Q \rightarrow Q)$	$+(I \rightarrow U \rightarrow Q)$	$+(I \rightarrow V \rightarrow Q)$
	$+(U \rightarrow I \rightarrow Q)$	$+(U \rightarrow Q \rightarrow Q)$	$+(U \rightarrow U \rightarrow Q)$	$+(U \rightarrow V \rightarrow Q)$
$Q_6 =$	$-(I \rightarrow I \rightarrow Q)$	$+(I \rightarrow Q \rightarrow Q)$	$+(I \rightarrow U \rightarrow Q)$	$-(I \rightarrow V \rightarrow Q)$
	$-(U \rightarrow I \rightarrow Q)$	$+(U \rightarrow Q \rightarrow Q)$	$+(U \rightarrow U \rightarrow Q)$	$-(U \rightarrow V \rightarrow Q)$
$Q_7 =$	$+(I \rightarrow I \rightarrow Q)$	$+(I \rightarrow Q \rightarrow Q)$	$+(I \rightarrow U \rightarrow Q)$	$+(I \rightarrow V \rightarrow Q)$
	$-(U \rightarrow I \rightarrow Q)$	$-(U \rightarrow Q \rightarrow Q)$	$-(U \rightarrow U \rightarrow Q)$	$-(U \rightarrow V \rightarrow Q)$
$Q_8 =$	$-(I \rightarrow I \rightarrow Q)$	$+(I \rightarrow Q \rightarrow Q)$	$+(I \rightarrow U \rightarrow Q)$	$-(I \rightarrow V \rightarrow Q)$
	$+(U \rightarrow I \rightarrow Q)$	$-(U \rightarrow Q \rightarrow Q)$	$-(U \rightarrow U \rightarrow Q)$	$+(U \rightarrow V \rightarrow Q)$
$U_5 =$	$+(I \rightarrow I \rightarrow U)$	$+(I \rightarrow Q \rightarrow U)$	$+(I \rightarrow U \rightarrow U)$	$+(I \rightarrow V \rightarrow U)$
	$+(U \rightarrow I \rightarrow U)$	$+(U \rightarrow Q \rightarrow U)$	$+(U \rightarrow U \rightarrow U)$	$+(U \rightarrow V \rightarrow U)$
$U_6 =$	$-(I \rightarrow I \rightarrow U)$	$+(I \rightarrow Q \rightarrow U)$	$+(I \rightarrow U \rightarrow U)$	$-(I \rightarrow V \rightarrow U)$
	$-(U \rightarrow I \rightarrow U)$	$+(U \rightarrow Q \rightarrow U)$	$+(U \rightarrow U \rightarrow U)$	$-(U \rightarrow V \rightarrow U)$
$U_7 =$	$+(I \rightarrow I \rightarrow U)$	$+(I \rightarrow Q \rightarrow U)$	$+(I \rightarrow U \rightarrow U)$	$+(I \rightarrow V \rightarrow U)$
	$-(U \rightarrow I \rightarrow U)$	$-(U \rightarrow Q \rightarrow U)$	$-(U \rightarrow U \rightarrow U)$	$-(U \rightarrow V \rightarrow U)$
$U_8 =$	$-(I \rightarrow I \rightarrow U)$	$+(I \rightarrow Q \rightarrow U)$	$+(I \rightarrow U \rightarrow U)$	$-(I \rightarrow V \rightarrow U)$
	$+(U \rightarrow I \rightarrow U)$	$-(U \rightarrow Q \rightarrow U)$	$-(U \rightarrow U \rightarrow U)$	$+(U \rightarrow V \rightarrow U)$